Available online at www.sciencedirect.com
SCIENCE DIRECT®
Journal of Sound and Vibration 288 (2005) 235–254
JOURNAL OF SOUND AND VIBRATION
www.elsevier.com/locate/jsvi

# On the noise transmission and control for a cylindrical chamber core composite structure

Deyu Li, Jeffrey S. Vipperman*

*Department of Mechanical Engineering, University of Pittsburgh, 648 Benedum Hall, 3700 O'Hara Street, Pittsburgh, PA 15261, USA*

Received 26 January 2004; received in revised form 22 November 2004; accepted 5 January 2005
Available online 17 March 2005

**Abstract**

The vibroacoustic properties, sound transmission behavior, and noise transmission control of a novel chamber core composite cylinder are studied. An approximate uniform shell model of the sandwich cylindrical chamber core structure is developed to aid in the calculation of the ring frequency and external critical frequency. Acoustic modal parameters are analytically and experimentally obtained. The structural modal parameters are identified from measured data. The coupling between structural and acoustic modes is investigated. The sound transmission into the cylindrical chamber core is experimentally characterized, where the stiffness-, cavity resonance-, mass-, and coincidence-controlled zones are identified. Finally, the addition of fills to the wall chambers of the chamber core is investigated as a part of passive control study, which also serves to corroborate the model development.


## 1. Introduction

Several novel composite structures have been investigated for expendable launch vehicles [1–7], which offer higher strength and stiffness, larger payload envelope, lighter weight, and better fabrication benefits than the aluminum structures that they replace. These advantages, however, are accompanied by an increase of sound transmission through the structures [8–10], which is

*Corresponding author. Tel.: +1 412 624 1643; fax: +1 412 624 4846.
*E-mail addresses:* deyul@hotmail.com (D. Li), jsv@pitt.edu (J.S. Vipperman).

0022-460X/$ - see front matter © 2005 Elsevier Ltd. All rights reserved.
doi:10.1016/j.jsv.2005.01.007

mainly governed by the dynamic properties of the structural acoustic system. Severe noise levels occurring during launch may damage the often fragile payload. Thus, mitigating noise transmission through composite structures is currently an important research topic.

The Air Force Research Laboratory, Space Vehicles Directorate, developed a Chamber Core composite structure (referred as to Chamber Core), which is a sandwich-type structure fabricated from multi-layered composite face sheets separated by channels that form passive acoustic chambers [7]. These acoustic chambers have the potential to create an acoustic resonator network that can be used to attenuate noise inside the closed Chamber Core cylindrical structure [1,7].

Previous studies of the Chamber Core have focused on optimal design, damage mechanisms, and fabrication methods [7,11]. The goals of this work are to characterize the noise transmission into this novel composite structure and determine if including passive fills in the wall chambers is an effective treatment to reduce internal noise levels during external sonification. Towards this end, some specific aims include: (1) experimental measurement of the noise transmission through the structure; (2) determination of the structural acoustic resonance frequencies and their impact on the noise transmission; (3) examination of the effects of ring, external coincidence, and internal coincidence frequencies on the noise transmission properties of the structure, and (4) corroboration of noise transmission regions, as well as the ring and coincidence frequency prediction models using results obtained from the passive control study.

The paper is organized into seven sections. Section 2 presents a simplified uniform cylindrical shell model for the Chamber Core, which is used to predict some important structural acoustic frequencies. Section 3 presents results from structural–acoustic modal identification, including the impact of the coupling between the modes of the structure and the acoustic cavity. In Section 4, the behavior of sound transmission into the cylindrical Chamber Core is experimentally characterized, and four distinct regions of the noise transmission spectrum are identified. The passive control study is presented in Section 5, the results of which are used to validate the four regions of the transmission spectrum as corroborate the models that predict the ring and external critical frequencies in Section 6. Finally, the conclusions are given in Section 7.

## 2. Structural acoustic frequencies

Three special frequencies, including the ring frequency, cutoff frequencies, critical (external and internal for a thin-wall cylinder) frequencies are of interest to describe the sound transmission behavior of a cylindrical shell [13]. The calculation of ring frequency and external critical frequency is based on an isotropic uniform shell. The effective uniform cylindrical shell of the sandwich-type Chamber Core is developed by means of the equivalent of bending stiffness and mass (see Fig. 1). The technique permits the effective thickness and effective density of the uniform shell model to be determined. The thin-wall box-beam is used to calculate the bending stiffness of the sandwich-shell, which was used by George et al. [11] to optimize the wall thickness of the cylindrical Chamber Core.

The geometric dimensions including effective thickness, $h_{\text{eff}}$, are defined in Table 1. It is assumed that the outer and inner skins of the Chamber Core have the same thickness, $t_1$, and that the two sidewalls of each chamber have the same thickness, $t_2$. If the thickness of the two skins is much less than the distance between their surface, i.e. $t_1 \ll d$, the bending stiffness of the box-beam

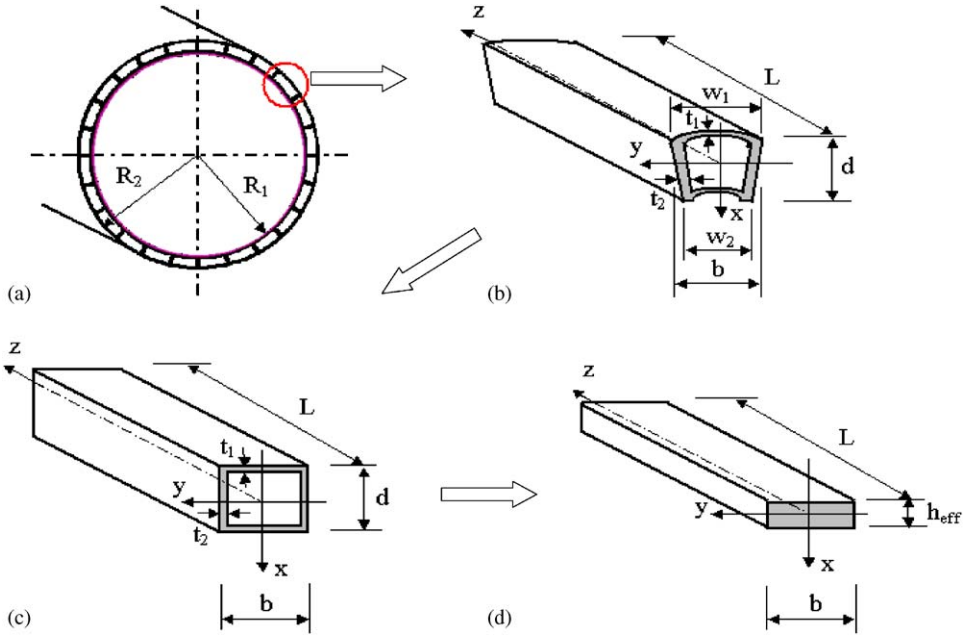


Fig. 1. Box-beam geometry: (a) Chamber Core cylinder, (b) one wall Chamber section, (c) equivalent square box-beam, (d) equivalent uniform solid beam.

Table 1
Physical and geometric parameters of the Chamber Core structure

| Material parameters | Geometric parameters (mm) | Effective parameters |
|---|---|---|
| $E_{\text{average}} = 60\,\text{GPa}$ | $R_1 = 255.0$ | $h_{\text{eff}} = 4.1\,\text{mm}$ |
| $\mu_{\text{average}} = 0.3$ | $R_2 = 275.0$ | $\rho_{\text{eff}} = 1554.7\,\text{kg/m}^3$ |
| $\rho_{\text{shell}} = 1494\,\text{kg/m}^3$ | $L = 760.0$ | |
| $\rho_{\text{air}} = 1.21\,\text{kg/m}^3$ | $w_1 = 72.0$ | |
| $c = 346\,\text{m/s}$ (at 75 °F) | $w_2 = 66.6$ | |
| | $b = 69.4$ | |
| | $d = 25.8$ | |
| | $t_1 = 1.7$ | |
| | $t_2 = 1.3$ | |

can be approximated as [12]

$$EI_{yy} \approx \frac{Ed^2(3t_1b + t_2d)}{6(1-\mu^2)}, \tag{1}$$

where $b = (w_1 + w_2)/2$ is the average widths of the wedge box-beam, and $w_1$ and $w_2$ are the width of the top and bottom sides of the wedge-box-beam (see Fig. 1b), respectively. $E$ is Young's modulus, $\mu$ is Poisson's ratio, and $I_{yy}$ is the moment of inertia around $y$-axis. The effective

thickness, $h_{\text{eff}}$, is calculated when the bending stiffness of a uniform beam ($EI_{yy,\text{uniform}} = Eb h_{\text{eff}}^3/12$) is the same as that of the box-beam given by Eq. (1), or

$$h_{\text{eff}} \approx d\sqrt[3]{\frac{1}{1-\mu^2}\left(\frac{6t_1}{d}+\frac{2t_2}{b}\right)}. \tag{2}$$

The effective density, $\rho_{\text{eff}}$, can be obtained in a similar manner from equating the equivalent mass per unit length of the uniform beam and the box-beam:

$$\rho_{\text{eff}} = \frac{2(t_1 b + t_2 d - 2t_1 t_2)\rho_{\text{shell}} + (w_1 + w_2 - 4t_2)(d - 2t_1)\rho_{\text{fill}}/2}{b h_{\text{eff}}}, \tag{3}$$

where $\rho_{\text{shell}}$ and $\rho_{\text{fill}}$ are, respectively, the density of the cylindrical shell and any fill media included in the cylinder wall chambers. The material properties and geometric parameters are shown in Table 1. The effective thickness and effective density are also given in the last column of Table 1. Average properties for $E$, $\mu$, and $\rho$ are used (homogenous properties).

After developing the uniform cylindrical shell, the ring frequency, critical frequency (external and internal), and cutoff frequencies can be predicted by the classic formulas [13], which are

$$f_R = \frac{c_p}{2\pi a}, \quad f_{\text{Cr\_ext}} = \frac{c^2}{2\pi}\sqrt{\frac{m}{B}}, \quad f_{\text{Cr\_int}} = 1.8412\frac{c}{2\pi a}, \quad f_{\text{Cut}}^{lm} = \frac{k_r^{lm} c}{2\pi} \quad \text{(Hz)}, \tag{4–7}$$

where $f_R$ is the ring frequency, $f_{\text{Cr\_ext}}$ the external critical frequency, $f_{\text{Cr\_int}}$ the internal critical frequency, and $f_{\text{Cut}}^{lm}$ the cutoff frequency; $c_p$ is the speed of sound propagating in a flat panel of the same thickness and material as the cylindrical shell, which is calculated by $c_p = \sqrt{E/\rho(1-\mu^2)}$, and $a$ is the radius of the cylinder. $m = h\rho$ is the surface area density of the shell, $B = Eh^3/12(1-\mu^2)$ the flexural rigidity of the plate of the same material and thickness, and $c$ the speed of sound. $k_r^{lm}$ is the radial wavenumber which can be solved from the boundary conditions [13], $l$ the number of radial pressure nodes, and $m$ the number of diametral pressure nodes.

The material properties of the Chamber Core are as follows: the average isotropic Young's modulus, which is obtained from a parametric FEA study of a structure made from identical graphite–epoxy material in Refs. [5,6] is $E = 60\,\text{GPa}$, Poisson's ratio is selected as $\mu = 0.3$, and the density of the skin material is measured as $\rho = 1494\,\text{kg/m}^3$. The geometric dimensions of the cylindrical Chamber Core shell are given in Table 1. The ring frequency, cutoff frequency and internal and external critical frequencies of the cylindrical Chamber Core are calculated and listed in Table 2.

Table 2
Ring, cutoff, critical frequencies of the Chamber Core system

| Parameter | Value (Hz) |
|---|---|
| Ring frequency, $a = R_1$ | 3911 |
| Cutoff frequency | 398 |
| Internal critical frequency | 398 |
| External critical frequency | 2478 |

## 3. Identification of structural/acoustic modal parameters

The sound is transmitted into the cylinder by means of the interaction between structural and acoustic vibration. Thus, the structural and acoustic modal parameters are the basic physical quantities to characterize the noise transmission into the cylindrical enclosure. The measurement systems for identifying the modal parameters of the structural and acoustic system are as follows. The diagram of the measured structure and the coordinate system used is shown in Fig. 2. Heavy square plates constructed from two layers of 1.9-cm-thick medium density fiber (MDF) boards are installed at the two ends of the Chamber Core cylinder and sealed with Armaflex® insulation. A boom is designed and installed to hold the internal microphones. A Kenwood™ loudspeaker (KFC-W2000) is mounted at the bottom of the Chamber Core cylinder to excite the cavity modes. The frequency response functions between the speaker and microphones are measured to identify the acoustic modal parameters. Impact tests are also conducted in order to experimentally determine the structural modal parameters. A PCB model 086C03 modally tuned hammer is used to excite the structure while an array of 6 PCB 352B22 0.5-g accelerometers measured the response at various locations.

In order to examine the effects of the structural resonances on the acoustic resonances, the analytical method [14] is used to calculate the natural frequencies of the acoustic cavity under the assumption of rigid enclosure walls. These results are then compared with the experimentally identified ones to determine the extent of the effect of the structural modes on the acoustic modes. The analytical mode numbers are given in the first column of Table 3, and the analytical natural frequencies ($f_{ANA}$) below 1000 Hz are listed in the fourth column of the table.

The acoustic modal parameters (natural frequencies and damping ratios) of the Chamber Core are identified from measured data. A total of 48 acoustic measurements are taken with the internal

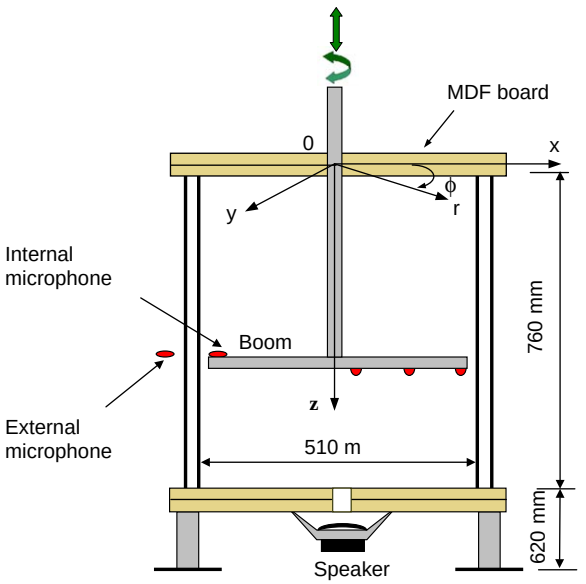


Fig. 2. Schematic diagram of the Chamber Core cylindrical fairing.

Table 3
Acoustic modal parameters of the cavity enclosed in the Chamber Core structure

| Mode shape order (*l,m,n*) | Measured frequency (Hz) | Measured damping ratio (%) | Analytical frequency (Hz) |
|---|---|---|---|
| 001 | 227.8 | 0.54 | 227.6 |
| 010 | 398.4 | 0.67 | 397.6 |
| 002 | 451.9 | 0.57 | 455.3 |
| 011 | 458.1 | 0.45 | 458.2 |
| 012 | 603.4 | 0.36 | 604.4 |
| 020 | — | — | 659.6 |
| 003 | 682.2 | 0.24 | 682.9 |
| 021 | — | — | 697.7 |
| 013 | 789.4 | 0.25 | 790.2 |
| 022 | 803.7 | 0.31 | 801.4 |
| 100 | 837.5 | 0.25 | 827.5 |
| 101 | 866.6 | 0.32 | 858.2 |
| 030 | 905.6 | 0.21 | 907.3 |
| 004 | 911.5 | 0.24 | 910.5 |
| 031 | — | — | 935.4 |
| 102 | — | — | 944.4 |
| 023 | 951.4 | 0.33 | 949.4 |
| 110 | 987.6 | 0.30 | 993.6 |

microphones positioned at combinations of the following coordinates: $r = \{55, 145, 235\}$ mm, $\phi = \{0^\circ, 30^\circ, 60^\circ, 90^\circ\}$, and across vertical planes at $z = \{120, 240, 360, 480\}$ mm. The FRFs at different excitation positions are also measured in order to find as many acoustic modes as possible. A curve fit is simultaneously performed on 48 selected frequency response functions for acoustic modal frequency and damping identification. A representative acoustic frequency response function and its curve fit at $(r, \theta, z) = (235\,\text{mm}, 30^\circ, 240\,\text{mm})$ are shown in Fig. 3. The identified acoustic natural frequencies and damping ratios are given in Table 3, which are also indicated in Fig. 3 as vertical dashed lines.

By comparing the identified natural frequencies with the analytical results listed in columns 2 and 4, respectively, of Table 3 it is observed that no extraneous modes are found, which suggests that the "structurally dominant" modes have little impact on the observed acoustic response—a consequence of the relatively high damping in the structure, which is given in Table 4. It is also noted from Table 3 that the 020, 021, 031, and 102 "acoustically dominant" modes are missing in the identified results and thus were likely not well-excited by the loudspeaker.

In order to identify structural modal parameters, a continuous area on the shell surface is selected, in which 48 measurement points are distributed. Different driving points are also used to provide additional insight. A curve fit is performed on the measured frequency response functions between these inputs and response locations in order to extract global natural frequency and damping ratios. A representative FRF curve at $(r, \theta, z) = (275\,\text{mm}, 0^\circ, 240\,\text{mm})$ is shown in Fig. 4, where the vertical dotted lines indicate the structural resonant frequencies, and the dark color regions are where the acoustically dominant modes impact the structural FRF. From the measured structural frequency response functions, it is observed that there are peaks at 395, 454, 794 Hz,

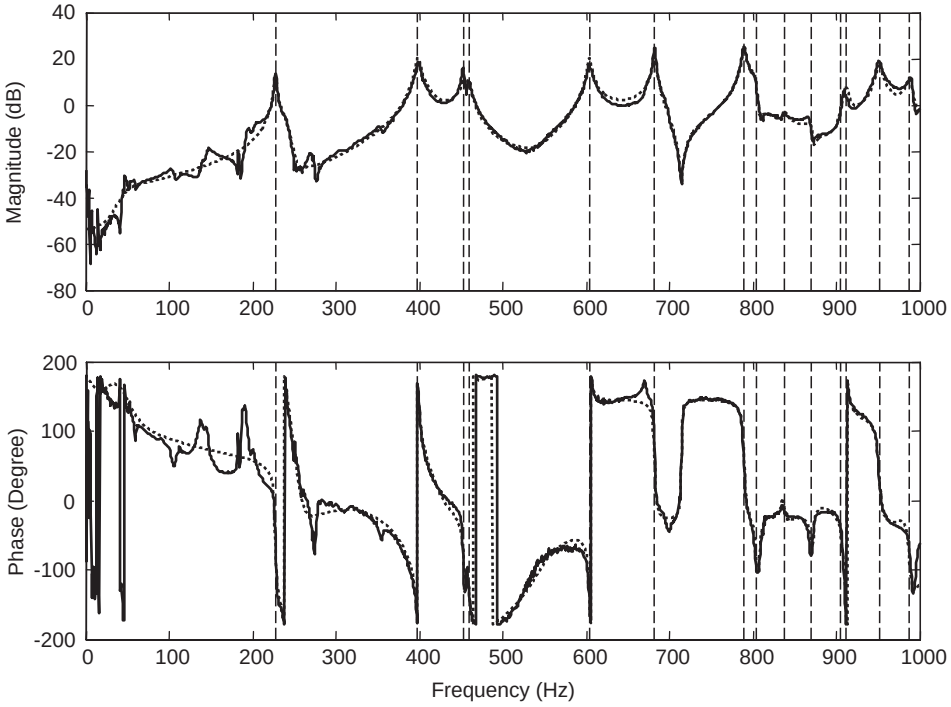


Fig. 3. Measured (——) and modeled (· · · · ·) representative acoustic cavity FRF between a microphone at (235 mm, 30°, 240 mm) and a speaker at (245 mm, 45°, 760 mm). The acoustically dominant resonance frequencies are denoted with dashed vertical lines.

Table 4
Measured structural modal parameters of the Chamber Core structure

| Mode no. | Measured frequency (Hz) | Damping ratio (%) |
|---|---|---|
| 1 | 242.1 | 9.91 |
| 2 | 272.4 | 1.00 |
| 3 | 306.4 | 3.29 |
| 4 | 346.6 | 2.06 |
| 5 | 499.7 | 1.26 |
| 6 | 552.1 | 0.90 |
| 7 | 570.1 | 1.69 |
| 8 | 628.0 | 2.42 |
| 9 | 672.5 | 1.54 |
| 10 | 705.7 | 1.96 |
| 11 | 736.6 | 1.88 |
| 12 | 747.1 | 1.00 |
| 13 | 853.0 | 0.82 |
| 14 | 877.3 | 1.13 |

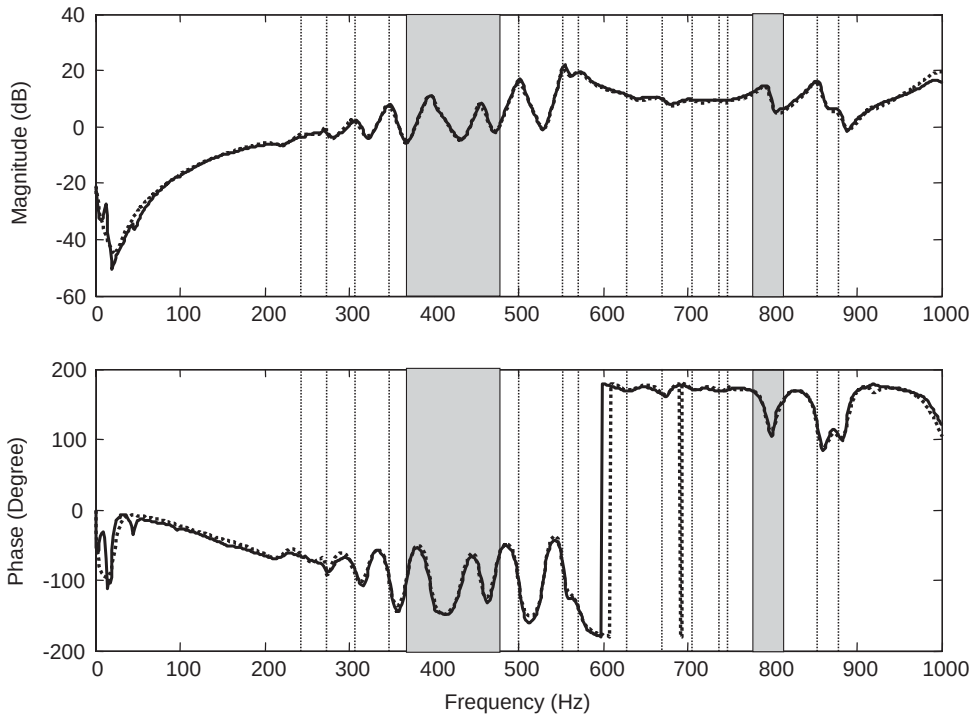


Fig. 4. Measured (——) and modeled (· · · · ·) representative structural FRF between an accelerometer at (275 mm, 0°, 240 mm) and an impact hammer at (275 mm, 0°, 240, 540 mm). The shadowed areas indicate regions with acoustic effects.

which are close to the "acoustically dominant" cavity resonances at 398 Hz (010 mode), 452 Hz (002 mode), 790 Hz (013 mode), respectively. Inspecting the measured structural frequency response functions, it is found that these peaks are not real structural resonances, but the coupled effect of the acoustic cavity resonances on the structure. When the impact hammer drives the shell, the internal acoustic cavity is also excited by the vibrating shell. Because the acoustic damping is very small, the fluid loading at the excited resonances is relatively high, which reacts with the shell to create the coupled structural vibration. The identified structural modal frequencies and damping ratios are given in Table 4. From Table 4 it can be seen that the structural damping is relatively high for the composite structure due to voids and other defects. Therefore, structural damping treatments are not expected to provide significant attenuation in noise transmission into the cylinder.

## 4. Sound transmission into the Chamber Core cylinder

The sound transmission loss (TL) through a structure is determined by physical properties of the structure, such as mass, stiffness, and damping ratio, and provides useful information for the noise transmission control. In order to characterize sound transmission through cylindrical shells, Holmer and Heymann [15] defined a sound power transmission coefficient to be equal to the ratio

of power radiated per unit surface area of shell to the power passing axially through a unit area of cross section. In other Refs. [16–19], researchers suggested using the noise reduction instead of calculating transmission loss, which was defined as the ratio of outer time- and surface-averaged mean-square pressures to inner time- and volume-averaged mean-square pressures. The above two methods of characterization are difficult to implement in measurement. In this study, an in situ method was used to characterize broad-band sound transmission into a cylindrical structure [1,6,20]. It is also called noise reduction (NR), which is computed as

$$\mathrm{NR}(\omega) = -10\log_{10}\frac{\langle p_{\mathrm{int}}^2(\omega)\rangle}{\langle p_{\mathrm{ext}}^2(\omega)\rangle}, \tag{8}$$

where $\langle p_{\mathrm{ext}}^2(\omega)\rangle$ is the mean-square external pressure spectrum averaged over the outside shell surface, and $\langle p_{\mathrm{int}}^2(\omega)\rangle$ is the mean-square internal pressure spectrum averaged over the inside shell surface.

Four speakers (KLH-9912, bandwidth: 28–20,000 Hz) driven by Marchand PS-24 power amplifiers are arranged around the Chamber Core and excited with independent white noise sources having a bandwidth of 0–20,000 Hz in order to simulate a diffuse field. Note that finite cylinders are reported not to suffer from directionality in their sound transmission spectrums as is observed in infinite cylinders [18]. The external speakers are suspended 620 mm above the floor. An internal B&K Type 4190 microphone is installed at one end of a boom 245 mm from the central axis, and a corresponding outer microphone (B&K Type 4190) is installed that is 15 mm from the surface of the cylinder shell (see Fig. 2). All signals are generated and measured using a Siglab MC20-84 dynamic signal analyzer. Fig. 5 depicts a top view of this measurement setup.

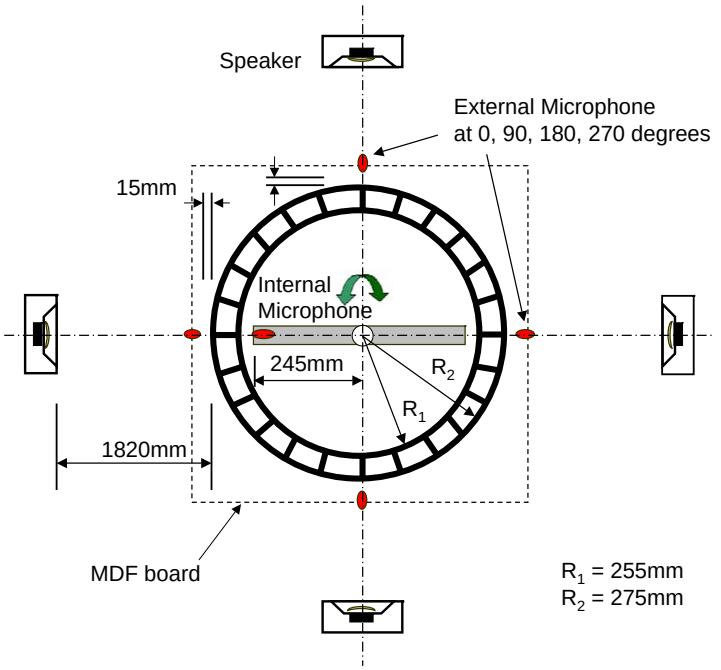


Fig. 5. Top view of NR measurement setup.

The internal microphone records internal measurements that are at the same height and angles as the exterior measurements. The two microphones traverse to 24 different measurement locations around the Chamber Core. The 24 locations for the Chamber Core cylinder span across six different vertical heights, $h = \{120, 240, 360, 480, 600, 720\}$ mm, and four different transverse angles $\phi = \{0^\circ, 90^\circ, 180^\circ, 270^\circ\}$.

The experimental results of the NR for the Chamber Core are shown in Figs. 6 and 7. In Fig. 6 a linear frequency axis from 0 to 1000 Hz is used. The analytical cavity resonance frequencies (dash-dotted vertical lines) and the measured structural resonance frequencies (dashed vertical lines) are shown in the figure so that the effects of the acoustic and structural resonances on the NR can be examined. Several observations from Fig. 6 are made, as follows

(1) There is a dip around 50 Hz. It is likely the "Helmholtz frequency" that results from the imperfect sealing of the Chamber Core. From 100 Hz to the first cavity resonance, 227.6 Hz, the noise reduction is seen to be roughly 35 dB, but fluctuates $\pm 5$ dB.

(2) Significant dips in the NR are noted at most of the cavity resonance frequencies (227.6, 397.6, 455.3, 458.2, 604.4, 659.6, 682.9, 697.7, 790.2, 801.4, 827.5, 907.3, 910.5, 935.4, 944.4, 949.4, and 993.6 Hz), which are indicated by dash-dotted, vertical lines.

(3) The structural resonances are found not to produce significant dips in the NR with the exception of the ninth structural resonances at 672.5 Hz, which is in proximity to acoustic modes at 659.6 and 682.9 Hz.

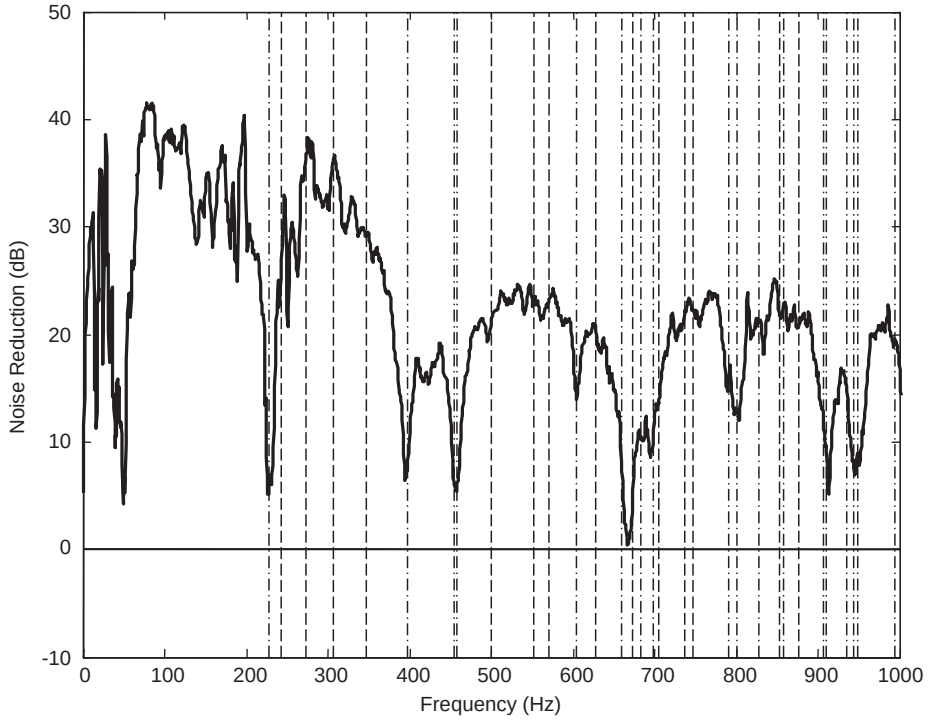


Fig. 6. Measured NRS of the Chamber Core structure. Vertical lines indicate structural (– – – –) and acoustic (– · – · –) resonance frequencies.

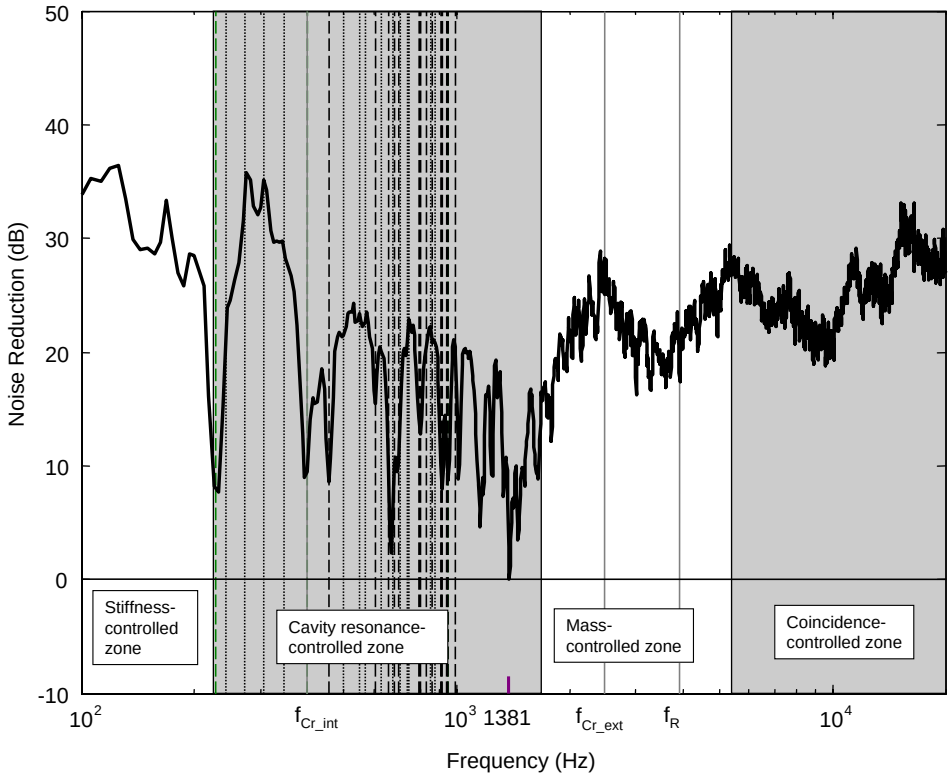


Fig. 7. Measured NR and important structural acoustic frequencies of the Chamber Core structure with four zones identified.

(4) The minimum value of the NR in [0, 1000] Hz occurs at 666.8 Hz. The acoustic resonances at 659.6 Hz (020 mode) and 682.9 (003 mode) and the structural resonance at 672.5 Hz contribute to this dip. Because the damping ratio in this particular structural mode is large (1.54%), the sound radiation from the damped structural mode is limited. However, considering the strong effects of other cavity modes and given that the acoustic damping ratio is very small (0.24% at 682.9 Hz), it is expected that the contribution from the acoustic modes is much larger than that from structural mode.

(5) The measurement results show that the cavity resonances have the most influence on the NR in the frequency range 200–1000 Hz.

In Fig. 7, the NR is reploted with a logarithmic frequency axis having a larger frequency range of 100–20,000 Hz. The predicted ring frequency ($f_R$), external and internal critical frequencies ($f_{\mathrm{Cr\_ext}}$ and $f_{\mathrm{Cr\_int}}$) from Table 2 are indicated on the frequency axis as well as with solid vertical lines. It is observed that the NR curve has similarities with the noise transmission loss for a flat panel. Specifically, there are stiffness-, mass-, and coincidence-controlled zones in the NR curve, which are identified in Fig. 7. These zones will be experimentally verified later in this study. One difference between TL for a panel and NR for the cylinder is that there is an acoustic cavity resonance-controlled zone in the NR, which contains the significant effects of the acoustically

dominant resonances. Note that each zone will require different control strategies. To summarize the important observation about Fig. 7:

(1) The structural stiffness-controlled zone extends from 0 Hz to the first cavity resonance frequency, 227.6 Hz.

(2) The cavity resonance-controlled zone begins from the first cavity resonance at 227.6 Hz, and ends at the beginning of the mass-controlled zone at about 1600 Hz. In the cavity resonance-controlled zone, internal coincidence may occur, which was found in a previous study [6] to significantly worsen the noise transmission. It is predicted that the internal coincidence happens around 1381 Hz, which is also the frequency where the minimum value of NR occurs. Note that the frequency 1381 Hz is close to the analytical resonance frequency of 1385 Hz for the (050) acoustic cavity mode, suggesting that the coincidence occurring between the (050) acoustic cavity mode and the (50) structural shell mode significantly transmits noise into the Chamber Core cylinder.

(4) The mass-controlled zone occurs between 1600 and 5500 Hz. The dip in the mass-controlled zone is induced by the ring frequency, which is indicated in the figure by a solid, vertical line and the symbol $f_R$.

(5) Finally, the coincidence-controlled zone occurs above 5500 Hz. There are additional dips in the NR curve that are induced by external coincidence effects.

## 5. Passive noise transmission control

As part of a passive control study, five kinds of fill materials having different densities were added to the wall chambers of the cylindrical Chamber Core structure in order to investigate the effects on the NR. They are, in order of increasing density, (1) fiberglass (density 17.1 kg/m$^3$), (2) opened cell foam (density 32.0 kg/m$^3$), (3) perlite pellets (density 152.0 kg/m$^3$), (4) polyethylene pellets (density 544.0 kg/m$^3$), and (5) sand (density 1603.0 kg/m$^3$). Although the latter fills are too heavy to be practical, they do provide insight into the physical mechanisms of control. Figs. 8–12 show the controlled and uncontrolled NR when the wall chambers are filled with these five fills, and are again ordered from lightest to heaviest. For each of the figures, the solid line represents the NR for the empty wall chambers (air), and the dotted line indicates the NR for the cylinder when the wall chambers include the fill materials. The resulting structural acoustic frequencies, $f_{\mathrm{Cr\_int}}, f_{\mathrm{Cr\_ext}}, f_R$ are computed for each case (see Table 5) and shown in the figures as solid vertical lines.

In comparing Figs. 8–12, it is observed that the lighter fills (i.e. fiberglass and opened cell foam in Figs. 8 and 9) have little effect on the NR in the 200–1400 Hz (cavity resonance-controlled zone), because the small variation in density cannot significantly change the structural response, which provides the energy to excite the acoustic cavity. However, for the higher-density fills (i.e. polyethylene pellets and sand shown in Figs. 11 and 12), significant improvement is noted in the region of the cavity resonance-controlled zone of the NR that is closest to the mass-controlled zone (around the predicted internal coincidence frequency 1381 Hz). There may be two reasons for this effect: one is that the mass increase results in a significant reduction in the dynamic structural response; another is created by the effective increase in structural damping due to the interaction of the heavy pellets, which degrades the

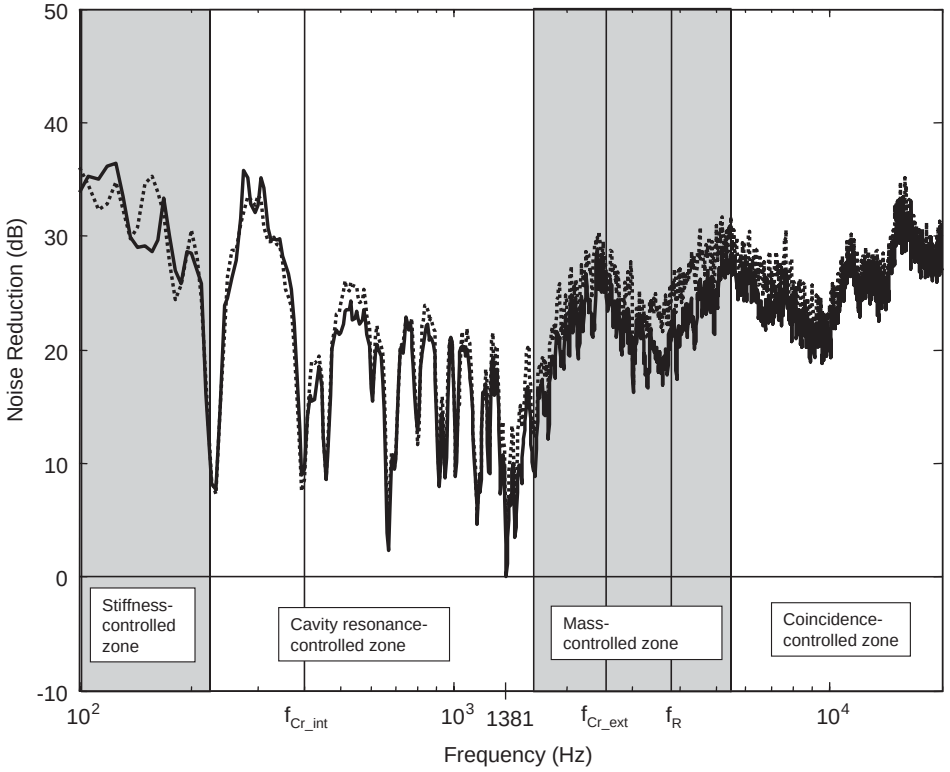


Fig. 8. NRS of chambers filled with air (——) and fiberglass (· · · · ·).

internal coincidence occurring between the (050) acoustic cavity mode and the (50) structural shell mode. One can also observe that as the fill density increases, improvement of the NR in the mass-controlled zone is significant; as much as 20 dB increase is observed and the mass-controlled zone enlarges (see Fig. 12). The start of the coincidence-controlled zone shifts towards the right as the mass-controlled zone enlarges, and the fluctuation in the NR curve in the visible part of the coincidence-controlled zone becomes smaller as the external critical frequency increases with increasing fill density. The onset of the coincidence-controlled region is approximately 5200 Hz in Fig. 7 (no fill) and increases to approximately 12,000 Hz for the heaviest fill presented in Fig. 12. Finally, when comparing the stiffness-controlled zones in Figs. 8–12, little difference is observed since the fills have little impact on structural stiffness.

In order to quantitatively analyze the effect of each of the five passive fills on the NR, the averaged NR reduction in each of the four NR regions is calculated and presented in Fig. 13. The "star", "sun", "triangle", and "heart" symbols with a short horizontal line indicate the averaged NR in the stiffness-, acoustic cavity resonance-, mass-, and coincidence-controlled zones, respectively. The air (no fill added), fiberglass, opened cell foam, perlite pellets, polyethylene pellets, and sand is indicated in the abscissa, respectively, in the order of increasing density.

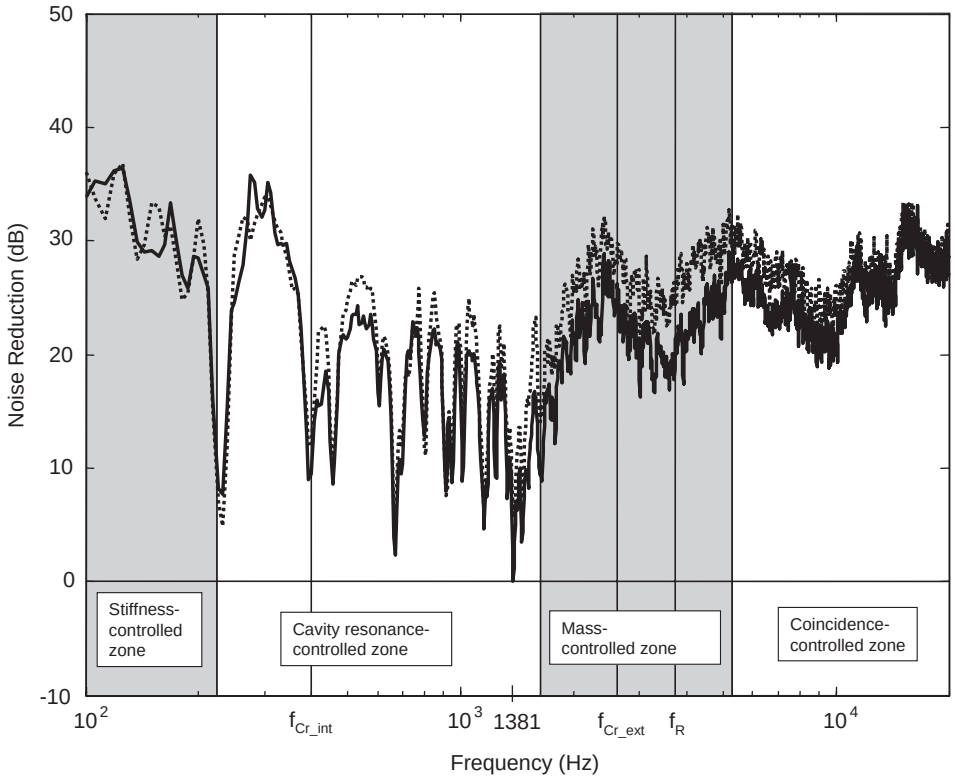


Fig. 9. NRS of chambers filled with air (——) and open cell foam (· · · · ·).

The averaged NR value (dB rms) is calculated using

$$\overline{\mathrm{NR}} = 10\log_{10}\left(\sum_{i=1}^{N} 10^{\mathrm{NR}(i)/10}\right), \tag{9}$$

where NR($i$) is the value of noise reduction at the $i$th frequency in each region. Note that the intervals for mass- and coincidence-controlled zones change for each case represented by Figs. 8–12.

The improvement in averaged NR is found to increase with the increasing density of the fill materials added to the cylinder wall chambers. In Fig. 13 it is observed from the star symbols that the averaged NR in the stiffness-controlled zone responds with modest improvements when fill materials are added. The averaged NR ranges from 47.0 to 50.8 dB as the density of fill increases from 1.2 kg/m$^3$ (air) to 1603.0 kg/m$^3$ (sand). A slightly more noticeable improvement in the NR is noted for the acoustic cavity resonance-controlled zone (heart symbols with short horizontal line). It is noted that the low-density materials (such as fiberglass and opened cell foam) have little effect on the NR in this region, however a maximum change of 5.9 dB is observed when sand is added. In contrast, a more significant effect on the mass-controlled zone of the NR (triangle symbols) is noted, as expected. The maximum increase in averaged NR is 20.9 dB when the heaviest fill (sand)

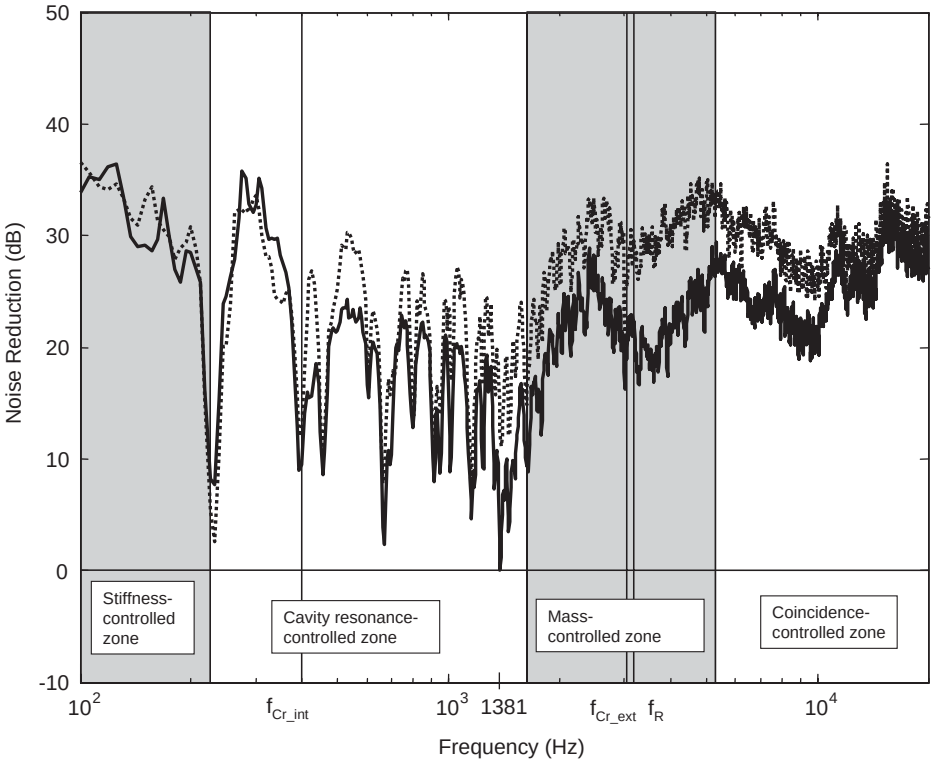


Fig. 10. NRS of chambers filled with air (——) and perlite pellets (· · · · ·).

is added. The sun symbols in the figure indicate the effects of the fill density on the NR in the coincidence-controlled zone, which are also significant. For this case, the maximum increase in averaged NR is 10.7 dB for the sand fill. All three of the higher-density fills (perlite pellets, polyethylene pellets and sand) are found to create significant improvement in the NR in coincidence-controlled zone.

Although the results of the passive control study are encouraging, the reader is cautioned that significant reductions were only achieved for very dense fills (polyethylene and sand), where the mass contributions are impracticable. Further, most of the control occurred in the mass- and coincidence-controlled regions ($>1000$ Hz), where the internal absorptive treatments for expendable launch vehicles are already effective [10]. In particular, the passive fills were found to have very little effect at the acoustically dominant cavity resonance frequencies below 1000 Hz. One study [21] noted that filling the cylindrical cavity entirely with expanded polystyrene packing fill can effectively remove the effects of the cavity acoustics. It is interesting to note that the results of Fig. 13 reflect the type of average result that could be expected from an statistical energy analysis (SEA) study, yet from Fig. 7, it is observed that significant dips in the NR can occur, e.g. at 1381 Hz, the structure is actually acoustically transparent (NR = 0). The study did however permit the verification of the four NR controlled regions, and the validation of the

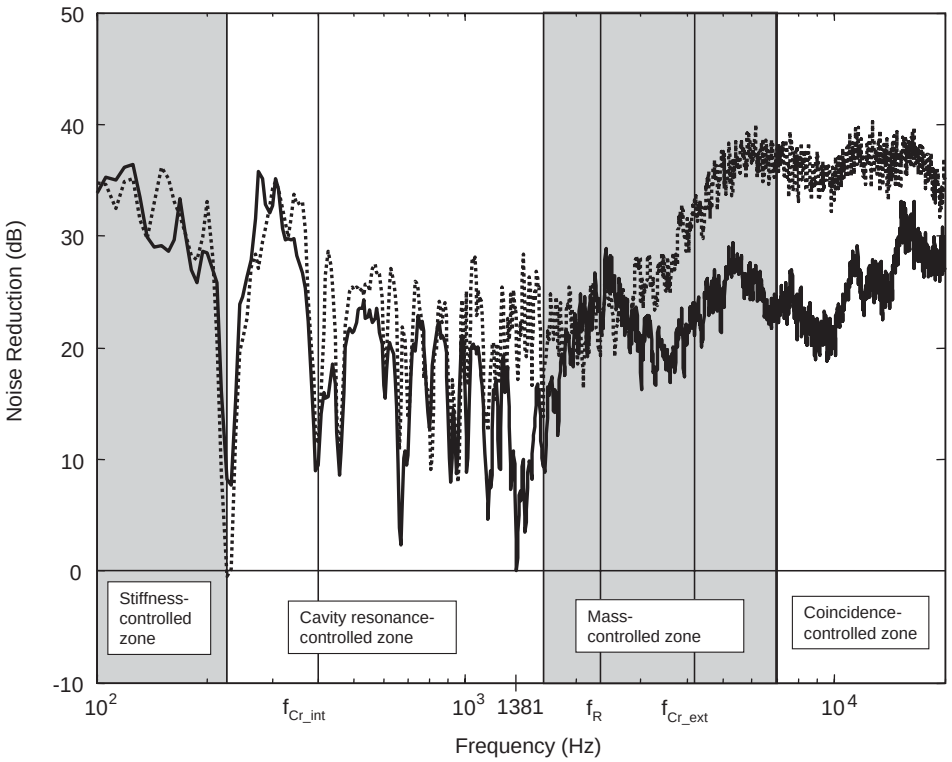


Fig. 11. NRS of chambers filled with air (——) and polyethylene pellets (· · · · ·).

approximations given by Eqs. (2) and (3), which were used to compute the special structural acoustic frequencies.

## 6. Verification of the NR regions and the effective model

The results of the passive control study are used to verify the four regions in the NR curves. In comparing Figs. 8–12 one can easily determine the range for each NR region. For example, the stiffness-controlled zone starts at 0 Hz, and ends at the first cavity resonance at 227.6 Hz. The acoustic cavity resonance-controlled zone starts from the first cavity resonance at 227.6 Hz, and ends near 1600 Hz. The width of mass-controlled zone increases as the effective density of the Chamber Core shell material increases. For the wall-chambers devoid of fill materials, the mass-controlled zone ranges across the interval of [1600,5500] Hz, above which the NR is controlled by coincidence phenomena. When the heaviest fill is added, this interval expands to [1600–12,000] Hz.

The results of passive control are also used to validate the structure model and the predicated ring and external critical frequencies. Table 5 gives the predictions of the ring and external critical coincidence frequencies, $f_R$, and $f_{Cr\_ext}$, which are dependent upon the effective shell thickness and density. When the average density increases from 1555 kg/m$^3$ (air filled) to 9985 kg/m$^3$

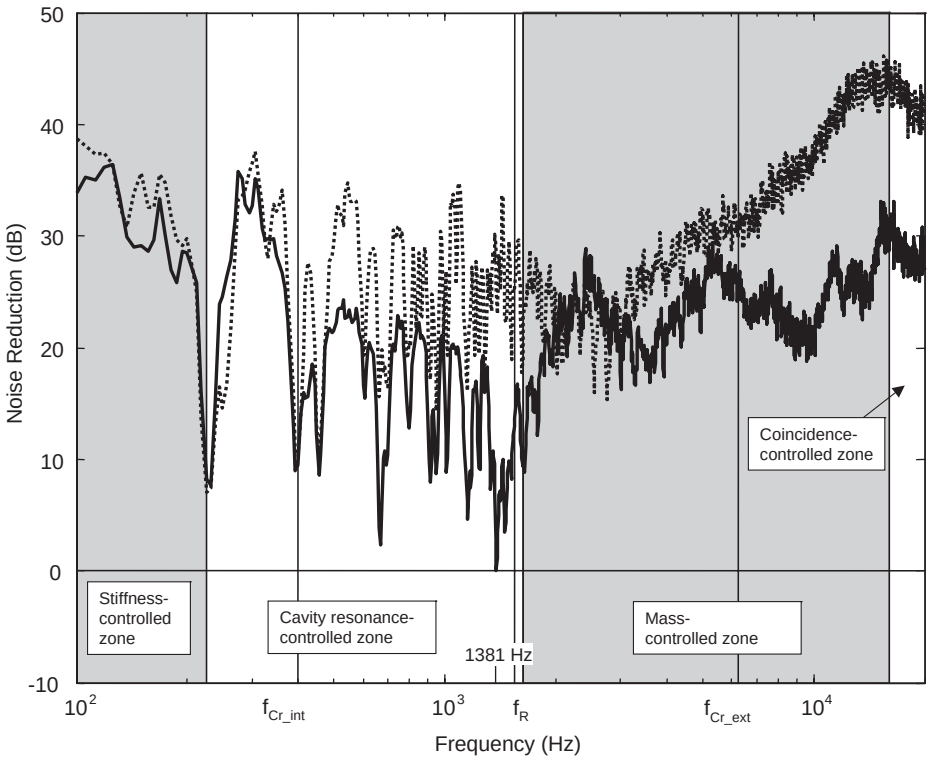


Fig. 12. NRS of chambers filled with air (——) and sand (· · · · ·).

Table 5
Density, ring and external critical frequencies of the chambers with/without fill

| | Fill density (kg/m$^3$) | Effective thickness (mm) | Effective shell density (kg/m$^3$) | Ring frequency (Hz) | External critical frequency (Hz) |
|---|---|---|---|---|---|
| Air | 1.2 | 20.1 | 1554.7 | 3911 | 2478 |
| Fiberglass | 17.1 | 20.1 | 1638.4 | 3810 | 2544 |
| Opened cell foam | 32.0 | 20.1 | 1716.8 | 3722 | 2604 |
| Perlite pellets | 152.0 | 20.1 | 2348.4 | 3182 | 3045 |
| Polyethylene pellets | 544.0 | 20.1 | 4411.6 | 2322 | 4174 |
| Sand | 1603.0 | 20.1 | 9985.4 | 1543 | 6280 |

(sand filled), the ring frequency drops from 3911 to 1543 Hz, while the external critical frequency increases from 2478 to 6280 Hz. These changes in $f_R$ and $f_{\mathrm{Cr\_ext}}$ are also denoted in Figs. 8–12 by solid vertical lines. Indeed, the dip noted near $f_R$ in the uncontrolled case given by Fig. 7 appears to track the changes in $f_R$ in Figs. 8–12. In addition, the secondary dips in NR, which occur above $f_{\mathrm{Cr\_ext}}$ also appear to track the changes in the external critical frequency. For example, in the absence of fill materials, $f_{\mathrm{Cr\_ext}} = 2478$ Hz while the secondary dips occur near 6000 Hz, or 2.4

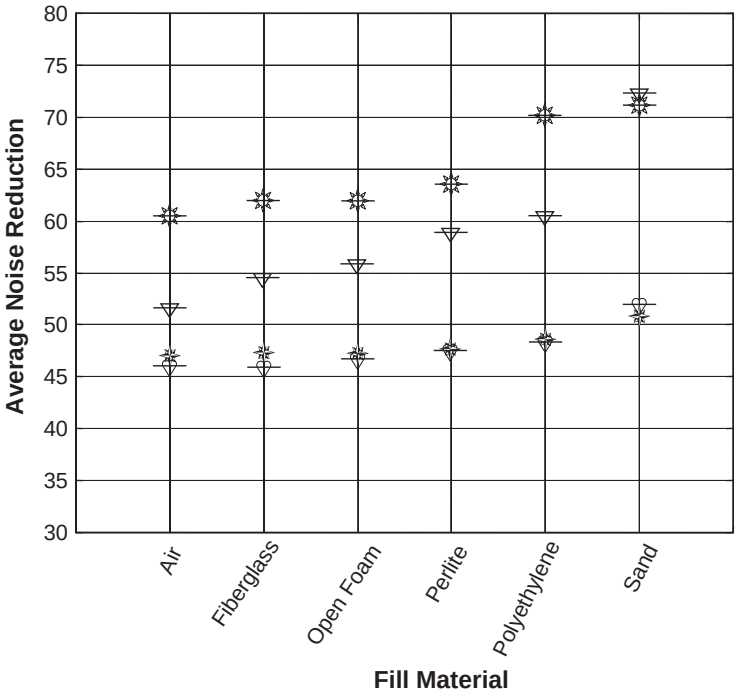


Fig. 13. Averaged NRS in the stiffness-controlled zone (✳), acoustic cavity resonance-controlled zone (▽), mass-controlled zone (▽), and coincidence-controlled zone (✳).

times the critical frequency, as shown in Fig. 7. In Fig. 12, the "smooth region" extends from $f_R$ at 1500 Hz out to secondary dips that occur around 15,000 Hz, which again is approximately 2.4 times $f_{\mathrm{Cr\_ext}} = 6280$ Hz. Similar trends are noted for the other fills given in Figs. 9–11.

## 7. Conclusions

The noise transmission into a novel Chamber Core composite structure has been experimentally characterized through noise reduction measurements and simplified models that predict the ring and external critical frequencies. Four distinct regions in the NR are identified: the stiffness-controlled, acoustic cavity resonance-controlled, mass-controlled, and coincidence-controlled. It was observed that the minimum values of noise reduction occurred at the acoustic cavity resonances, while the relatively highly damped structural modes of the Chamber Core had little apparent effect on the noise transmission.

An experimental passive noise transmission control study was conducted in order to evaluate the impact of adding various fill materials to the wall chambers of the Chamber Core cylinder. The results show that at high frequencies, i.e. in the mass-controlled and coincidence-control regions, significant increases in NR are observed with increasing density of the fill. However, adding the fills does not significantly improve NR in the low-frequency regions, where the NR is

dominated by the structural stiffness and acoustic cavity resonances. Since absorptive blankets already work well at high frequencies, the addition of fills in the chamber walls was found not to be a viable control strategy for expendable launch vehicles for the Air Force. While passive control methods were found to be infeasible due to the lack of impact on the acoustic cavity resonances, the results were used to validate the four NR regions and the ring and external critical frequency prediction models of the Chamber Core, which create dips in the high-frequency NR.

## Acknowledgments

The work was sponsored by the Space Vehicles Directorate, Air Force Research Laboratory (AFRL/VS). The POC for this effort is Dr. Steven A. Lane, and can be contacted at (505) 846-9944.

## References

[1] D. Li, Vibroacoustic Behavior and Noise Control Studies of Advanced Composite Structures, PhD Dissertation, School of Engineering, University of Pittsburgh, 2003.
[2] F. Shen, D. Pope, Design and development of composite fairing structures for space launch vehicles, *Society of Automotive Engineering Transactions* 99 (1) (1990) 1447–1455.
[3] S.M. Huybrechts, T.E. Meink, Advanced grid stiffened structures for the next generation of launch vehicles, *Proceedings of IEEE Aerospace Conference*, vol. 1, 1997, pp. 263–270.
[4] T.E. Meink, Composite grid vs. composite sandwich: a comparison based on payload shroud requirements, *Proceedings of IEEE Aerospace Conference*, vol. 1, 1998, pp. 215–220.
[5] J.S. Vipperman, D. Li, I. Avdeev, Investigation of the sound transmission into an advanced grid-stiffend structure, ASME IMECE 2001, Paper NCA-23539, New York, NY, November 11–16, 2001, pp. 1–8.
[6] J.S. Vipperman, D. Li, I. Avdeev, S.A. Lane, Investigation of the sound transmission into an advanced grid-stiffened structure, *Journal of Vibration and Acoustics* 125 (2003) 257–266.
[7] E. Herup, S. Huybrechts, S. Griffin, S. Tsai, Method of making composite ChamberCore sandwich-type structure with inherent acoustic attenuation, U.S. Patent No. 6,231,710 B1, 2001.
[8] S.T. Griffin, K.K. Denoyer, A. Das, Passive vibration isolation for payload containers, *Journal of Intelligent Material Systems and Structures* 10 (1) (1999) 83–87.
[9] N.W. Hagood, E.F. Crawley, Experimental investigation of passive enhancement of damping for space structures, *Journal of Guidance, Control, and Dynamics* 14 (6) (1991) 1100–1109.
[10] T.F. Bergen, D.L. Kern, Attenuation of the Cassini spacecraft acoustic environment, *Proceedings of the 1996 42nd Annual Technical Meeting of the Institute of Environmental Sciences*, 1996, pp. 254–265.
[11] T.J. George, M.-H. Herman Shen, S.M. Huybrechts, T.E. Meink, Optimal design of composite ChamberCore structures, *Composite Structures* 52 (3–4) (2001) 277–286.
[12] S.Y. Zhang, J.Q. Liu, X.X. Yu, L.W. Cai, *Mechanical Properties of Composite Structures*, Beijing Institute of Technology Press, Beijing, 1992.
[13] F. Fahy, *Sound and Structural Vibration: Radiation, Transmission and Response*, Academic Press, London, 1993.
[14] R.D. Blevins, *Formulations for Natural Frequency and Mode Shape*, Van Nostrand Reinhold, New York, 1979.
[15] C.I. Holmer, F.J. Heymann, Transmission of sound through pipe walls in the presence of flow, *Journal of Sound and Vibration* 70 (2) (1980) 275–301.
[16] L.R. Koval, Effects of cavity resonances on sound transmission into a thin cylindrical shell, *Journal of Sound and Vibration* 59 (1) (1978) 23–33.
[17] J.E. Manning, G. Maidanik, Radiation properties of cylindrical shells, *Journal of the Acoustical Society of America* 36 (9) (1964) 1691–1698.

[18] P.H. White, Sound transmission through a finite, closed, cylindrical shell, *Journal of the Acoustical Society of America* 40 (5) (1966) 1124–1130.
[19] L. Cheng, Fluid-structural coupling of a plate-ended cylindrical shell: vibration and internal sound field, *Journal of Sound and Vibration* 174 (5) (1994) 641–654.
[20] D. Li, J.S. Vipperman, Mathematical model for characterizing noise transmission into finite cylindrical structures, *Journal of the Acoustical Society of America* 117 (2) (2002) 679–689.
[21] D. Li, J.S. Vipperman, Noise transmission control study on a ChamberCore structure, *ASME IMECE Conference*, Paper IMECE02-33069, New Orleans, LA, November 17–22, 2002, pp. 1–8.